Enhanced Sea Ice Concentrations from Passive Microwave Data

Josefino C. Comiso
NASA Goddard Space Flight Center

1. Introduction

Sea ice concentration is usually defined as the fraction of ice covered area within an observational field, which in our case is the footprint of the satellite sensor. This assumes that the ocean surface is binary, i.e., either ice covered or ice free. With the binary characterization of the ice covered surface in mind, ice concentration can be quantified from satellite instrumental observations of the radiative flux, R, from the surface using a mixing algorithm given by

$$R = R_I C_I + R_O C_O \qquad (1)$$

where R_I is the radiation that is normally observed from 100% ice covered areas and R_O is the corresponding value of 100% open water while C_I and C_O are the concentrations for ice and water respectively. In principle, the equation is independent of sensor resolution and should provide similar results regardless of resolution.

The binary characterization of the surface is valid only if the observations allow this to be possible and the discrimination of sea ice and open water can be done unambiguously. This assumes that within the footprint of the sensor, the radiances from 100% ice and 100% liquid water are distinct enough to make it possible to estimate or infer from the data the concentration on a measurement by measurement basis. This is generally true for microwave data (and also for visible, infrared which are usually used for validation studies) but it is not always the case and there are at least two situations in which there is a special concern, namely: (a) new ice/thin ice regions as in polynyas and marginal ice zones during autumn and winter and (b) melt/meltponding regions as in Arctic basin during the spring and summer. In new/thin ice regions, the emissivity of sea ice is not well defined since it changes constantly from close to that of liquid water to that of thick sea ice. Other physical processes associated with the growth of sea ice that may affect the radiative signature are described in detail in Weeks and Ackley (1986), Tucker et al. (1992), and Eicken et al. (1991). Also, when the surface temperature goes above freezing in spring and summer, the brightness temperature of the surface goes up as the emissivity increases to almost that of a blackbody as liquid starts to form around the ice crystals, but as the snow continues to melt and forms slush and then melt ponds, the brightness temperature goes down to that of an ice free water (Eppler et al., 1992).

Despite these problems, ice concentration has became one of the most important parameters that have been used to study the large scale variability and characteristics of the global sea ice cover. It turned out that with passive microwave, we are able to map consistently, the location and distribution of the most dominant types of sea ice cover (i.e., young ice, first year ice and multiyear ice) with reasonably good accuracy. The data have been used successfully to estimate the extent and area of the sea ice cover (Gloersen et al., 1992; Parkinson et al., 1999; Zwally et al., 2002) and to make projections of

decadal trends (Comiso, 2002; Serreze et al., 2000; Stroeve et al., 2004). It has also been used to characterized the marginal ice zones and important ice features like polynyas and Odden (Comiso and Gordon; 1996; Comiso et al., 2001). Although errors in the ice concentration have been quantified and estimated to be from less than 5 to more than 15% (depending on surface conditions), interpretation of such errors is not trivial because the spatial distribution of the sea ice cover is much more complex that a binary distribution of either ice or water. For example, even in the simple case of an area covered mainly by consolidated ice but with recently formed leads in mid winter, there is already an interpretation problem. If the fraction of lead area is, for example, 10%, the estimated ice concentration should be 90%. This may indeed be the case if the satellite passes by the area at the time when the leads were forming and the emissivity of the lead is the same as that of open water. The emissivity, however, changes with time and when the satellite passes by the same area a few hours later, the same lead is likely covered by grease ice and then thin nilas in the following orbit with the emissivity of the surface constantly changing and significantly higher than that of open water. A daily average of measurements from the same area will thus likely provide an ice concentration that is different from 90% but the retrieved value would vary depending on whether an area covered by 100% grease ice is interpreted as 100% ice concentration or not. Such interpretation would make the ice cover in winter almost featureless. Users of passive microwave sea ice parameters should thus be aware about how the algorithms are formulated and understand what a retrieved 100% ice cover represents.

This document is meant as a guide for users of the recently released new ice concentration maps derived from an enhanced Bootstrap Algorithm as described in the following sections. In the Arctic, the changes are relatively minor compared to those released previously and consisted mainly in the adjustment of tie-points to get the retrieved values more consistent with validation data sets. In the Antarctic, the changes in technique are more significant with two sets of channels now being used, instead of one set, for improved accuracy and consistency with validation data. The change makes the Antarctic algorithm basically identical to that for the Arctic the main difference being in the input parameters. The results are very similar to those generated previously with the biggest change being a few percent increase in ice concentrations around the periphery of the Antarctic continent. While relatively small, the changes are considered important because of the special role of coastal polynyas, especially along the Antarctic coastline, in the formation of bottom water that drives the global thermohaline circulation. Inter-calibration and adjustments in the tie-points were also made with the ultimate intent of generating a consistently derived and accurate sea ice data set that can be used for variability and trend studies.

2. The Bootstrap Algorithm

According to the Rayleigh-Jeans approximation, electromagnetic radiation is linearly related to surface temperature at microwave frequencies and can be expressed in units of temperature which we call brightness temperature, T_B. Using equation (1), the sea ice concentration can be expressed simply as

$$C_I = \frac{T_B - T_o}{T_I - T_O} \qquad (2)$$

where T_O and T_I are the brightness temperatures of ice-free ocean and sea ice, respectively, and the concentration of ice free surface $C_O = 1 - C_I$. Equation (2) is the basic equation used by all sea ice concentration algorithms. The big challenge has been how to obtain good estimates of T_B, T_O and T_I which are functions of emissivity (ε), surface temperature (T_S), and atmospheric opacity.

An ideal algorithm for retrieving the ice concentration would be the one that calculates accurately the parameters T_B, T_O and T_I in equation (2) at each field-of-view of satellite observation. Again, this assumes that the surface of interest is binary and covered by a mixture of water and ice as represented by T_O and T_I, respectively The first parameters, T_B, is the satellite measurement but it needs to be corrected to account for atmospheric effects which can differ significantly from one measurement to another. This means that a radiative transfer equation must be used and the opacity τ of the atmosphere must be known when each measurement is made. T_O and T_I are radiometer measurements of open water and sea ice, respectively, but the ice parameter varies with ice type.

Earlier algorithms used radiosonne data at some Arctic regions and assumed constant atmospheric and surface conditions and the results provided good results regionally and for the period atmospheric data were available (Svendsen et al., 1983; Swift et al., 1985) but generally, there were problems when used as a global algorithm. The algorithms that are currently more frequently utilized are those that take advantage of the multichannel capability and use the satellite data for obtaining the required input parameters in equation (2) (e.g., Comiso et al., 2003). Two of these algorithms are the Bootstrap Algorithm and the Nimbus-7 Team Algorithm (now called the NASA team algorithm), both developed at the NASA Goddard Space Flight Center (Cavalieri et al., 1984; Comiso, 1986). The Bootstrap Algorithm took advantage of the unique distribution of brightness temperature (or emissivity) data points in two or three dimensional space to assess and evaluate the general distribution of consolidated ice and use the pattern to obtain the unknown values of T_I and T_O in equation (2). The original Team Algorithm used three tie points, namely, two for two ice types (i.e., first year and multiyear ice) and one for open water, and employs polarization and gradient ratios to minimize the effect of varying surface temperatures. The different techniques for accounting for spatial changes in ice temperature and emissivity and the use of different sets of channels yielded different results from the two algorithms (Comiso et al., 1997; Comiso and Steffen, 2002) in large areas of the polar regions. The different sensitivity of the different frequency and polarization channels to surface effects as discussed in Matzler (1984) has been assumed as the primary reason for the discrepancies in the retrievals. The original NASA Team Algorithm (now called NT1) has been substantially revised to make use of the 89 GHz in combination with other channels and is currently called NT2 (Markus and Cavalieri, 2000). With NT2, a radiative transfer model (e.g., Kumero, 1993) has to be used to correct for the high sensitivity of the 89 GHz data to atmospheric effects. It also requires some accounting on the large variations in the surface emissivity of sea ice at this frequency.

The Bootstrap Algorithm takes advantage of the unique clustering of data from consolidated sea ice regions in multichannel space (Comiso et al., 1984; Comiso and Sullivan, 1986; Comiso, 1986). The technique is schematically illustrated in Fig. 1. When the brightness temperatures (or emissivities) at one passive microwave channel are plotted versus those of another channel in ice covered regions (Fig. 1), most of the data points in the consolidated ice region where the concentration is about 95% or more are clustered along a line (i.e., AD). Also, most of the data points in the open ocean and also in ice free regions within the pack are clustered along OW (i.e., for certain sets of channels at different frequencies). The data points that represent ice free surfaces within the ice pack are the ones corresponding to the low brightness temperatures (or emissivities) near what is labeled as O since these are the ones that correspond to relatively calm surfaces. Waves and atmospheric disturbances over open ocean tend to increase the brightness temperature along OW. The spatial variation in ice emissivity is reflected by the range of the AD cluster along each coordinate which usually gets wider as the frequency gets higher. This is an indication that the key reason for the variability is the difference in scattering properties of the different surfaces due to different ice types and snow cover characteristics (Eppler et al., 1992; Grenfell, 1992). The scatter in the data points along AD is caused primarily by different emissivities for different ice types (e.g., first year and multiyear ice according to Vant et al., 1976). The variations across the line AD (i.e., width of the line) correspond primarily to spatial variations in surface ice temperature and atmospheric effects and provides a measure of the accuracy in the retrieval. The latter is minimized through the choice of optimal sets of channels as discussed below.

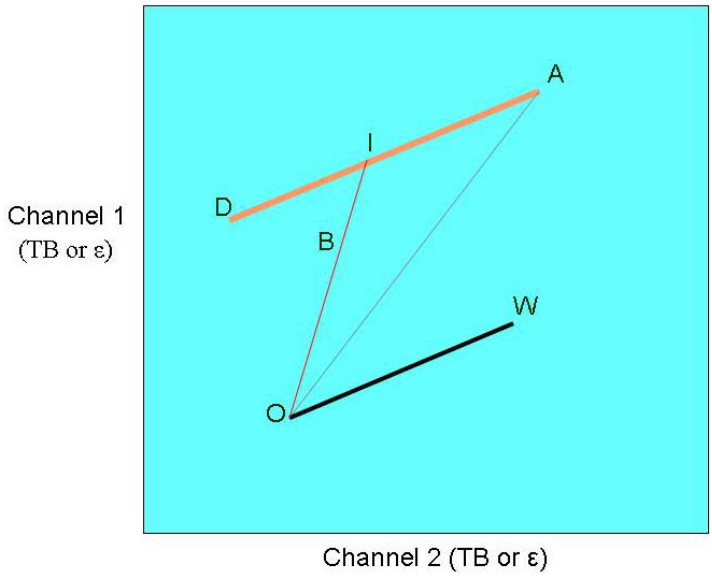

Figure 1 Schematic Diagram of the technique used by the Bootstrap Algorithm. the line AD represents consolidated ice while OW represents open water.

Two tie points for ice (AD) and water (O) are thus identified. Data points located between the line AD and O are interpreted as having ice concentrations between 0 and 100% in this scheme. Also, the variability in the emissivity (and temperature) of sea ice

is handled as follows. Note that for any type of ice surface represented by a data point I along the line AD, different concentrations of this ice type would be represented by data points along the line OI. Thus, given a data element at point B in the plot measured by the satellite sensor, the ice concentration can be derived by first extending the line along OB until it intersects the line AD. The intersection point, I, represents 100% ice for this particular ice type/surface and therefore T_I while O represents 0% ice and therefore T_O. Using this information using equation 2, ice concentration can be calculated. This can be done for either channels (along the horizontal or the vertical). but when T_O and T_I are close or equal to each other as can happen at 36 GHz (V) and higher frequencies, there is a singularity problem. Thus, the ratio of OB to OI is usually used, as described in Comiso (1995) which provides the same value as the ration of the numerator and denominator in equation 2. It should be noted that ice concentrations below a cut-off of about 10% are derived because the emissivities of ice and water are mainly impossible to discriminate at such values. The cut-off is made using the pattern associated with open water and is usually a line approximately parallel to OW. Further refinements are made using the 22 GHz channel as described in Comiso (1995).

The line AD is determined by the algorithm on a daily basis and inferred from a regression analysis of data points along the line. A small positive value of a few Kelvin is added to the offset of the regression line to account for the known presence of open water (of about 2 to 5%) for much of the consolidated ice regions. The estimate of the parameters of the line AD is critical to the accuracy of the ice concentration estimate. Part of the refinements in the enhanced version of the algorithm document is the optimization of the offset such that the retrieved ice concentration values are as consistent as possible with those from validation data sets (e.g., high resolution satellite data or detailed ship or aircraft observations).

Among the criteria for choosing the channels to be utilized are (a) they should provide the optimal resolution without sacrificing accuracy; and (b) ancillary data should be used only if necessary to improve accuracy. Thus, the set of 36 GHz channels (called HV36) is used because of reasonably good resolution and because the corresponding data in consolidated ice usually form a linear cluster with a well defined slope for AD (when one polarization is plotted versus the other) the value of which is approximately equal to one. The values form a linear distribution because the emissivity of ice is approximately the same for the two polarizations and they are affected by intermediary factors, like snow and the atmosphere, in much the same way. What makes it even more valuable is that the set is basically insensitive to spatial variations in temperature since the slope is approximately one and the change in brightness temperature in one channel due to temperature is approximately equal to that in the other channel. Thus the net effect of a changing temperature is to cause T_I to slide along the line AD and practically no impact on the accuracy in the retrieval of ice concentration. The sole use of 36 GHz channels provide some ambiguities since for this set of channels, the open ocean data cluster (i.e., the line OW) is either along the line OA in Figure 1 or to the left of this line. Furthermore, the horizontal channel is more sensitive to layering and other surface effects than the vertical channel (Matzler et al., 1984) and in some ice covered areas, the data points fall below or to the right of the line AD. Both problems are resolved through the

additional use of a set of channels that utilizes the 18 (or 19) GHz in combination with the 36 (or 37) GHz channel at vertical polarization (thereafter called the V1836 set) which provides an even easier discrimination and a good contrast between the emissivity of ice and water. Although the V1836 set provides a good mask for open ocean areas, the additional use of the 22 GHz channel significantly improves the effectiveness, as described in Comiso (1995). The use of the V1836 set shows some sensitivity to variations in surface temperature but the error introduced is estimated to be less than 3% because sea ice is usually covered by snow which is a good insulator and the observed standard deviation of ice temperatures is only about 2.5K.

Figure 2a is shown to illustrate how effectively the HV36 set of channels can be used to derive the sea ice concentration. The data points are from winter data in the Northern Hemisphere and the distribution for consolidated ice (in blue) is indeed quite compact and the slope is close to 1. The accuracy in the estimate of CI depends mainly on the accuracy in the estimate of T_I since it is known that T_I varies a lot more than T_O in the pack ice regions. The accuracy in the estimate of T_I is in turn dependent on how well AD represents 100% ice. The more well defined the linear cluster AD is the more accurate the retrieval is going to be. To quantify how well defined the ice cluster AD is, the scatter plot is rotated such that the AD cluster is along the vertical as shown in orange in Figure 2a. The width of the cluster can then be quantified with a frequency histogram of the sum of data points along the vertical within each horizontal bin as shown in Figure 2b. In the plot, the peak in the left correspond to the distribution of the data points of consolidated ice along an arbitray horizontal axis that can be converted to ice concentration since the relative location of TO is also shown in the plot (approximately the highest data point to the right). The standard deviation of the ice peak correspond to about 3% ice concentration. The uncertainty in the ice concentration associated with T_I is thus less than 3% since consolidated ice usually includes a fraction of open water within a relatively large footprint (which in this case is 25 by 25 km).

The only ancillary data used by the algorithm is climatological sea surface temperature which are used to mask out areas in the open ocean that are obviously ice free but not identified as such by the algorithm, despite the use of an ocean mask. The retrieval of sea ice at land/ocean boundary areas is also a problem for the algorithm since the emissivity of a mixture of land and ocean can be similar to that of sea ice. An algorithm originated by Cho et al. (1996) was modified and adapted to remove most of the problem areas but a final manual inspection of the daily maps is done to ensure that such source of error are minimize if not completely eliminated.

The Arctic and the Antarctic regions are quite different in that sea ice is surrounded by land in the Arctic while sea ice surrounds land in the Antarctic. In the winter, the Arctic is basically covered by consolidated ice that are more confined, thicker and colder that those in the Antarctic. In the Arctic, the ice floes can be as old as 7 years (Colony and Thorndike, 1988), while in the Antarctic, it is rarely the case that an ice floe is older than 2 years, the reason being that the remnants of summer ice gets flushed out of the original location by strong ocean currents (e.g., Weddell gyre) during autumn and winter. Also, there is more divergence in the Antarctic and no limit in the advance of sea ice in the

north because of the lack of a northern boundary. It is thus not surprising that the seasonality and microwave signatures of the sea ice cover in the two hemispheres are different and the signature of perennial ice is different in the Antarctic compared to that in the Arctic (Vant et al., 1976). To account for differences in physical and radiative characteristics, different algorithms are used to process the two hemispheres. The difference originally includes a difference in formulation but now, it is primarily the use of different input parameters for the two regions to optimize accuracy, as discussed below.

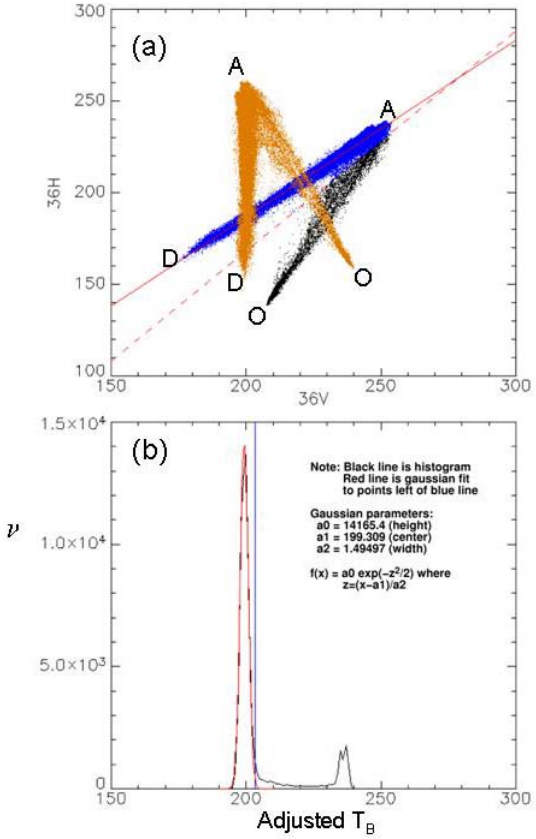

Figure 2. (a) Scatter plot of 36 GHz(V) versus 36 GHz(H) brightness temperatures with the ice cluster along AD shown as blue data points. Also shown is the same set of data points with the line AD along the vertical (in orange). (b) distribution of data points in (a) but with the AD ice line rotated and oriented along the vertical.

Only about 15% of the winter ice cover in the Southern Hemisphere survives the summer to become perennial ice but even the latter apparently have signatures similar to that of seasonal ice (Zwally et al., 1983; Gloersen et al., 1992). This is in part because second year ice appears to have signatures closer to that of first year ice than those of the multiyear ice in the central Arctic. The earlier version of the Bootstrap algorithm took advantage of this and for simplicity and convenience, utilized only one set of channels (i.e., the V1836 set) in the retrieval of ice concentration. Validation studies indicated that the use of this set of channels was adequate (Comiso et al., 1984; Comiso and Sullivan, 1986; Comiso and Steffen, 2003). However, this set of channels is known to be more vulnerable to temperature effects and new ice and these effects became more apparent in

the 1990s when big icebergs calved from the coastal areas and were subsequently grounded near the coast contributing to the formation of new ice in larger regions. New and young ice without snow cover can also have extremely cold temperatures (compared to average ice temperatures) in these regions in winter and therefore could cause large bias in ice concentration than usual. Comparative studies with satellite visible and infrared high resolution data, the coverage of which became more extensive and the data more readily available in recent years, indicated that the retrieved values using the original algorithm for the Antarctic has a negative bias of a few percentage ice concentration. It also became apparent that such bias is removed if an algorithm that is similar to that used in the Arctic (or a combined use of V1836 set and the HV36 set of data) is utilized. This makes sense since the HV36 is less vulnerable to temperature and new ice effects (because of shorter wavelength of the 36 GHz compared to that of the 18 GHz). This change actually constitutes the biggest change in the revised version of the Bootstrap data set.

The advent of the AMSR-E data in May 2002 provided an opportunity to investigate improvements through the use of the 6 GHz channel for retrieving the surface temperature of the ice as described in Comiso et al. (2003) and Comiso (2004). It turned out that this technique provided results that are almost identical to those of the original algorithm and it is not obvious whether the difference represents an improvement through the use of the 6 GHz channel or caused by an additional error associated with poorer resolution (of the 6 GHz) and uncertainties in the estimated emissivity of sea ice at 6 GHz and hence of the estimate of ice temperature.

The use of the basic algorithm (that does not use the 6 GHz) also enables retrieval from AMSR-E data of higher resolution ice concentration maps and hence now used as the standard. The 6 GHz channel, however, provides the largest contrast in the emissivity of sea ice and open water and can be used to evaluate the results from the algorithms. An ice concentration map was generated using the original Antarctic algorithm but using the 6 GHz (V) instead of the 19 GHz (V) in combination with the 37 GHz (V) data and presented in Figure 3a. The same set of data using the 19 GHz (V) as in the original algorithm is presented in Figure 3b. The two maps are almost identical and varies only by a few % ice concentration near the continent. For comparison, the enhanced version of the ice concentration map, using the new Antarctic algorithm, as presented in Figure 3c, shows a significantly different ice concentration distribution especially near the coastal regions. Since Figure 3b is basically unchanged even if spatial changes in ice temperature is taken into account, using the 6 GHz data, it appears that the difference between Figure 3b and 3c, may be associated primarily with new ice formation since the 37 GHz radiation is less penetrating than the 19 GHz and hence less sensitive to new ice surfaces. But further studies are needed to resolve the cause of this effect. While Figure 3c agrees better with visible and infrared data (e.g., MODIS) it should be pointed out that sea ice in the Antarctic is very dynamic as in areas where the difference between Figure 3b and 3c are largest as indicated by time series of NSCAT data. Also wind can be very strong in the region and new ice can be immediately covered by blown snow to make it look like thick ice in the visible images.

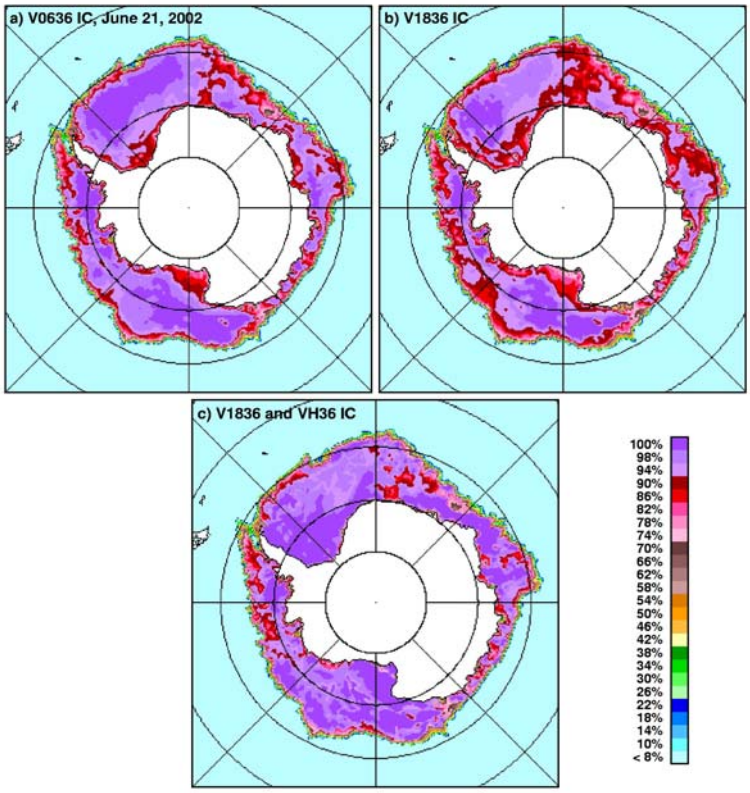

Figure 3. Sea ice concentration maps using (a) one set of channels, namely 6 and 18 GHz at vertical polarization; (b) one set of channels, namely, 18 and 37 GHz at vertical polarization; and (c) two sets of channels: one using 18 and 37 GHz at vertical resolution and the other using 37 GHz at both vertical and horizontal polarization.

3. Consistent Time Series of Passive Microwave Sea Ice Data

Change studies, especially in relation to climate, require as long historical record as possible. Unfortunately, current record on global sea ice cover data has not been that long since such data did not exist until the advent of the satellite era. The era started with the Nimbus-5/Electrically Scanning Microwave Radiometer (ESMR) which was launched in December 1972 and was the first microwave imaging (or scanning) system. The sensor is a one-channel system with a peak frequency of about 19 GHz and acquires data at variable incidence angles (since scanning is done cross-track). Because of the shortcomings of a one-channel sensor in providing ice concentrations, the series did not actually start until the advent of multichannel sensor with the launch of SMMR in October 1978. The SMMR sensor was succeeded by a series of SSM/I sensors that continues on to this day. The launch of AMSR-E in May 2004 started a new era of even more accurate ice concentration products at a significantly higher resolution (Comiso et al., 2003).

To create the time series of sea ice data we first tried to make sure that data from the different sensors that are as consistent as possible. In particular, we made the brightness temperatures (TBs) for the different sets of channels used to generate the ice concentration maps to match to each other as closely as possible. This in part minimizes effects of inconsistent calibration, incident angle, and peak frequency. Since AMSR-E

data provides the most accurate ice concentration to data, we use the data as the baseline. Thus, we first made SSM/I TBs to be consistent with those of AMSR-E TBs for each set of channels by normalizing the values of the former using parameters derived from linear regression of data from the two sensors during overlap periods. This was followed by making data from the different SSM/I sensors consistent and after that by getting the SMMR TBs consistent with SSM/I TBs. The next step is to use same sea ice concentration algorithm (i.e., the Bootstrap Algorithm as indicate above) for data from all sensors. Although it is the same formulation, the Bootstrap Algorithm will be called ABA when applied to AMSR-E data and SBA when applied to SSM/I data. Finally, the same techniques are used for the land mask, ocean mask, and land/ocean boundary masks as described in Comiso (2004) when generating the ice concentration maps.

To illustrate how well we succeeded with the aforementioned strategy, ice concentration maps from AMSR-E and SSM/I on 15 February 2003 in the Northern Hemisphere and on 15 September 2003 in the Southern Hemisphere are shown in Figure 4. In general, the technique appeared to have worked very well with the resulting daily ice concentration maps from different sensors showing very good agreement during overlapping periods. There are subtle differences especially near the ice margins associated with differences in resolution and antenna patterns of the different sensors but ice concentration values in practically all regions are virtually identical.

The good agreement in ice concentration is encouraging since it means that the same features of the ice cover are reproduced by the different sensors. The minor differences, which are mainly confined near the marginal ice zones, are inevitable because of innate differences in resolution, the peak frequencies for the radiometer channels used in the algorithm, the incident angle and the antenna side lobes. To gain insight into these differences, we first examine the procedure for masking open ocean areas which is

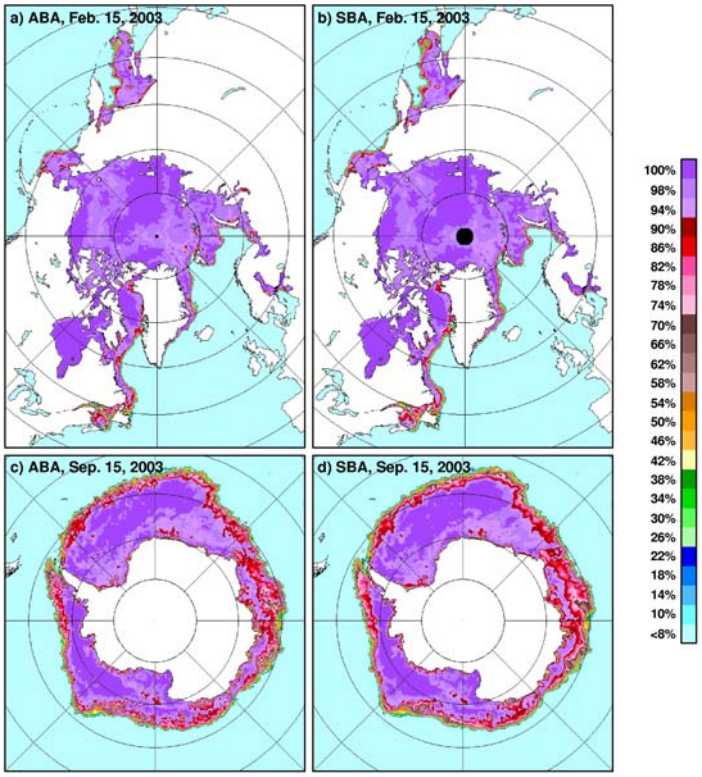

Figure 4. Daily ice concentration maps during winter in the (a) Northern Hemisphere using AMSR-E data; (b) Northern Hemisphere using SSM/I data; (c) Southern Hemisphere using AMSR-E data; and (d) Southern Hemisphere using SSM/I data.

basically done by setting a threshold below which the data is considered as open ocean.

The large contrast of the passive microwave signature of sea ice and open water at some of the channels has enabled estimates of the ice concentration at almost all values except at some low ice concentration values where the signature of open water and ice covered surfaces are virtually identical, as indicated earlier. Moreover, areas in the open ocean that are under the influence of abnormal weather conditions can have signatures similar to those of ice covered ocean. The use of a combination of 19, 22, and 37 GHz channels for the sensors, however, allows for effective discrimination of open ocean data under unusual conditions as illustrated in the scatter plots in Figure 5. In figures 5a and 5b, we show scatter plot of TB(19,V) versus the difference TB(22,V) – TB(19,V) using SSM/I and AMSR data, respectively, while in figures 5c and 5d, we show the corresponding plots but of TB(19,V) versus TB(37,V). The blue data points in the scatter plot along OW actually represent data from the open ocean at all weather conditions while the black data points are those from ice covered ocean. Open water within the pack is usually relatively calm and provides the lowest emissivity of data points along OW and is therefore represented in the algorithm as a data point close to the label O. In the open ocean the surface gets disrupted occasionally by strong winds and bad weather causing big waves and foam, which in turn cause the signature to move to higher values and towards W in the scatter plot, depending on the strength of the disruption. In the algorithm, data points along OW are masked to represent open water only with the red line, representing approximately 10% ice concentration used as the threshold as described

in Comiso et al. (2003). To obtain consistent ice extent and ice area from SSM/I and AMSR-E data, it is thus important to have the same threshold for both sensors. The set of data points between O and W which are considered as open water areas and should be separated from the ice covered surfaces with 10% ice concentration and above in the same way.

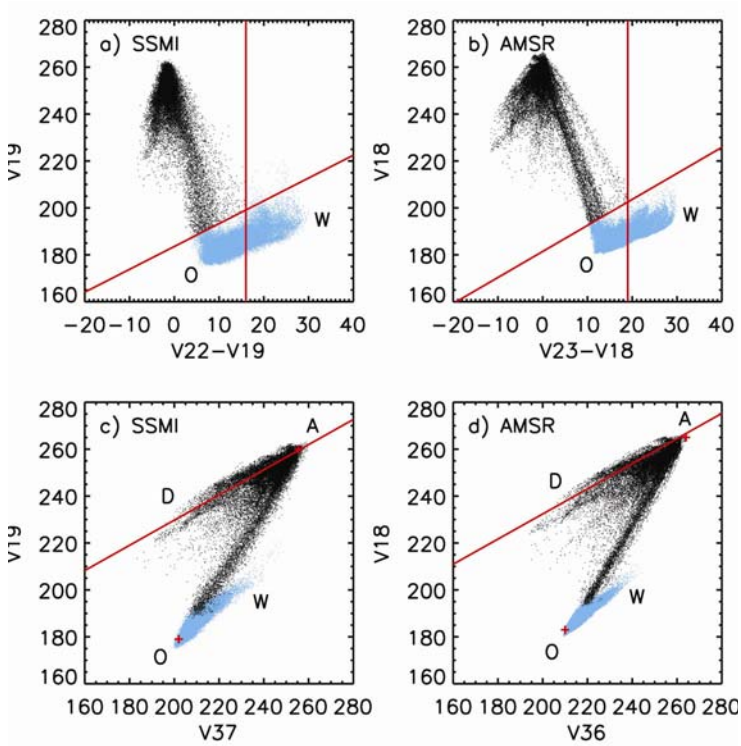

Figure 5. Scatter plots of TB(V19, V) versus TB(22, V) - TB(19, V) for (a) SSM/I and (b) AMSR-E data. Also, scatter plots of TB(19,V) versus TB(37,V) for (c) SSM/I and (d) AMSR-E data.

The higher resolution of AMSR provides a better definition of the marginal ice zone and a more precise location of the ice edge as previously indicated by Worby and Comiso (2004). This is clearly illustrated in the plots of brightness temperatures at different frequencies across the marginal ice zone (i.e., 35^{o} W longitude) in the Antarctic for both AMSR and SSM/I (Figure 6). The plots show that the brightness temperatures are relatively low and uniform in the open water (left side) and gradually increase over the marginal ice zone and reached their highest values over the consolidated ice region. Over the marginal ice zone that includes the ice edge, the changes in TBs are coherent and consistent at all AMSR-E frequencies. The TBs are not so consistent in the characterization of the ice edge for the different SSM/I channels (not shown). The corresponding plots for ice concentration, as shown in Figure 6c, indicate that AMSR-E provides a more defined ice edge than SSM/I with the latter further away from the pack by about 12 km. Such discrepancy makes it almost impossible to get a perfect match in the estimates of ice extent using data from the two sensors as will be discussed later.

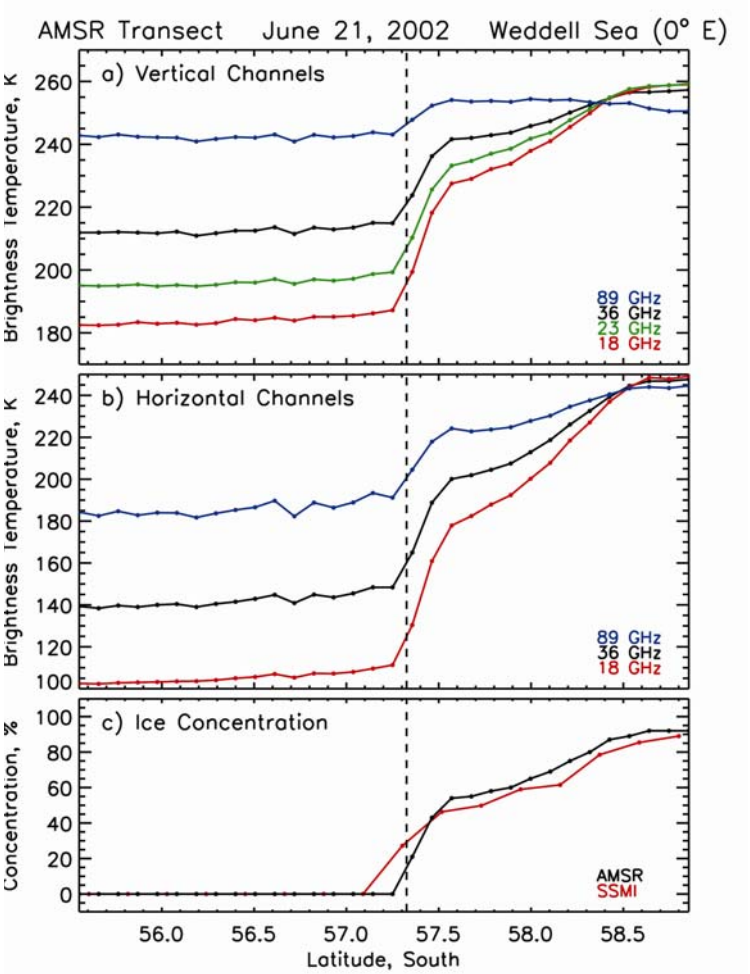

Figure 6. Transects along the ice edge of brightness temperatures using AMSR-E (a) vertically polarized and (b) horizontally polarized data and (c) comparison of ice edges as inferred from ice concentration values of AMSR-E and SSM/I.

Similar plots for ice concentration in the Barents Seas in the Northern Hemisphere along the 35 ^{o}E and 45 ^{o}E longitudes (not shown) show basically the same effect but sometimes, the differences are more modest. It is apparent that a bias exists, with the SSM/I data showing a location of the ice edge that is further away from the pack than the AMSR-E data. This phenomenon is associated with differences in resolution and side lobes of the antenna. The coarser the resolution is, the more the ice covered areas overlap with the open ocean. The effect of the antenna sidelobe is to cause a smearing at the ice edge since higher brightness temperature is observed as the satellite crosses the ice edge from the pack to the open ocean than vice versa. Such smearing is more pronounced with the SSM/I than the AMSR-E data which has a narrower field-of-view (and higher resolution) than the former.

4. Comparison of Sea Ice Extents, Area and Ice Concentration during Overlap Periods

The ice parameters derived from satellite ice concentration data that are most relevant to climate change studies are sea ice extent and ice area. Ice extent is defined here as the integrated sum of the areas of data elements (pixels) with at least 15% ice concentration while ice area is the integrated sum of the products of the area of each pixel and the corresponding ice concentration. Ice extent provides information about how far north the ice goes in winter and how far south it retreats towards the continent in the summer while the ice area provides the means to assess the total area actually covered by sea ice, and also the total volume and therefore mass of the ice cover, given the average thickness. In the previous section we discussed the technique we used for obtaining consistent ice concentrations from the various sensors. We now show how consistently we can get the ice extent and ice area from these sensors as well as average ice concentrations during periods of overlap. Figures 7a-7f show distributions of daily average ice extent, ice area and ice concentration over an entire annual cycle using AMSR-E and SSM/I data in 2005 for both Northern and Southern Hemispheres. The plots in Figures 7a and 7b show that the extents derived from SSM/I data (in blue) are consistently higher than those from AMSR-E data (in red) with the difference in winter relatively smaller than those in the summer period. The plots in Figures 7c and 7d show that the ice areas derived from SSM/I are still higher but much more consistent with those derived from AMSR-E data. These results suggest that the mismatch in resolution affects estimates of the extent more than the ice area with the coarser resolution system (i.e., SSM/I) providing the higher extent because of smearing effect as described earlier. The average ice concentrations from AMSR-E (Figures 7e and 7f) are also shown to be consistently higher by about 1 to 2% than that of SSM/I. This in part made the ice area from the two sensors more compatible. The main reason for the difference in extents from the two sensors is that there are more data elements with ice for SSM/I than AMSR-E, mainly because the ice edges in the former extends further beyond the MIZ than the latter, as discussed earlier. These additional data elements have low concentration values the inclusion of which causes the average ice concentration for the entire ice pack to be lower. The additional low ice concentration data also makes the average ice concentration lower for SSM/I than AMSR. The discrepancy is not so apparent with the ice area because the ice concentrations maps (see Figure 4, for example) basically match each other and the contribution of low concentration pixels at the ice edge is not as significant for ice area as with the ice extent estimates.

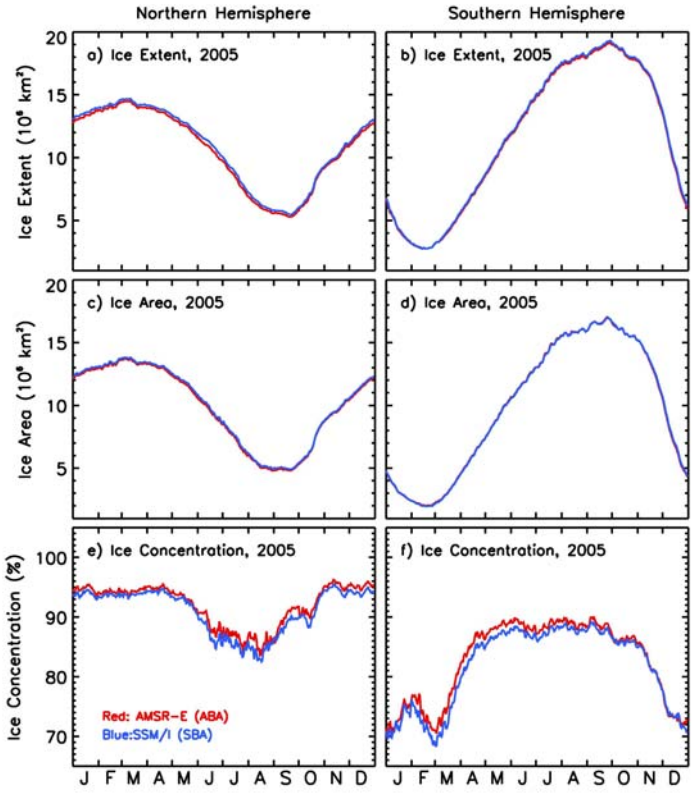

Figure 7. Daily ice extents (a &b), ice area (c & d), and ice concentration (e & f) during a period of SSM/I and AMSR-E overlap (2005) in the Northern and Southern Hemispheres

Similar comparative analysis of ice extents, ice area and ice concentration using data from two SSM/I sensors (i.e., F11 and F13) during the period of overlap from May to September 1995 is presented in Figure 8. The plots show very good agreement of data from the two sensors. This is not a surprise since the two sensors have virtually the same attributes. Slight differences in ice concentration estimates occur (e.g., 20 July 1995) but this may be associated with radiometer noise. It should be noted, that the good agreement was obtained after the two sensors were intercalibrated and the TBs were made consistent. Although the resolutions of F11 and F13 are expected to be the same, consistency in the derived ICs is needed to get consistency in the extent and area.

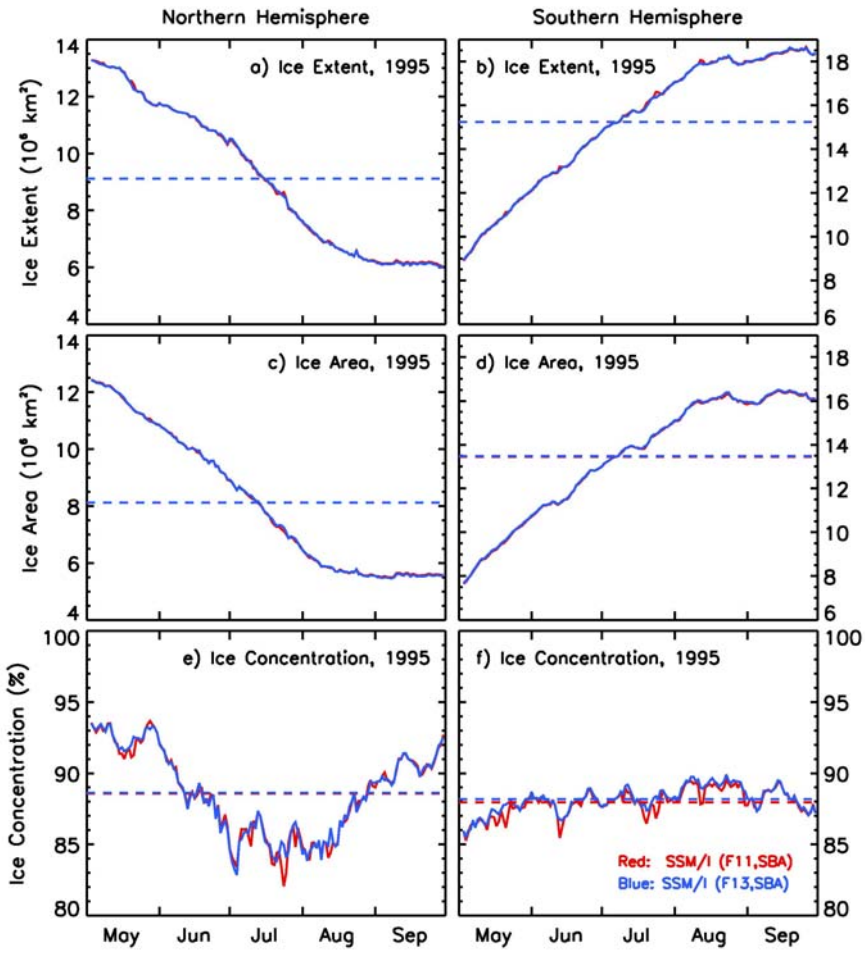

Figure 8. Daily ice extent (a &b), ice area (c & d), and ice concentration (e & f) during a period of SSM/I (F11) and SSM1(F13) overlap (May to September 1995) in the Northern and Southern Hemispheres.

During the overlap of SSM/I and SMMR data in mid July to mid-August in 1987 the extents and areas are also in relatively good agreement (Figure 9) during this summer period in the Arctic and the winter period in the Antarctic. It is interesting to note that the agreement was better during August than in July in the Northern Hemisphere but the opposite is true in the Southern Hemisphere. Also, the SSM/I values tend to be higher than those of SMMR in the Northern Hemisphere in July while the reverse is true in the Southern Hemisphere in August. Furthermore, the differences in the average ice concentrations are larger in the Northern Hemisphere than in the Southern Hemisphere and in July, SSM/I values are higher than those of SMMR while the opposite is true in July of the Southern Hemisphere. Because of these inconsistencies, it is not easy to establish whether there is a bias or not, especially since the overlap period is quite short.

Degradation in the quality of the SMMR data was occurring during this period and it is likely that the SMMR observations were not as accurate as those of SSM/I. An overlap of at least one annual cycle would have been desirable if only to establish that the seasonal differences are similar to those shown in Figure 9. In the time series that requires monthly averages, SMMR data were used to generate monthly data for July 1987 while SSM/I data were used for the August monthly. This procedure appears good for

the Antarctic data since there is good consistency of the two sensors in this region in July but such advantage is not as apparent in the Northern Hemisphere.

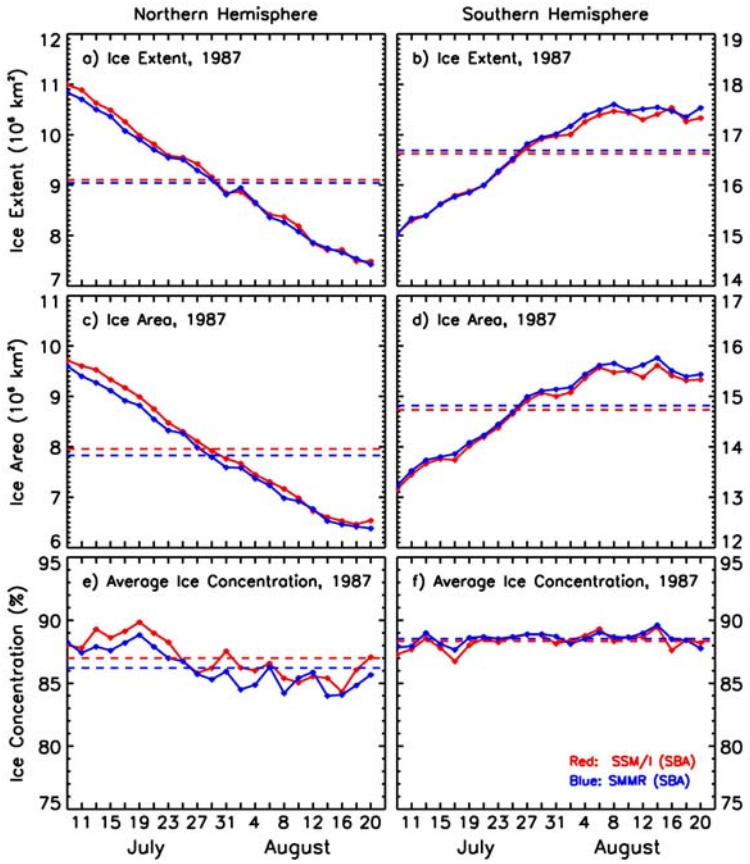

Figure 9. Daily extent (a &b), ice area (c & d), and ice concentration (e & f) during a period of SMMR and SSM/I operlap in the Northern and Southern Hemispheres (July to August 1987).

5. Summary

The new data set on ice concentration using an enhanced Bootstrap Algorithm is the result of a dedicated effort to generate a consistent and accurate time series of ice cover data. The project includes the use of the AMSR-E data set which is currently the best sea ice data available as the baseline for creating a consistent data set. The time series generated consists of SMMR data from November 1978 to August 1987, and SMM/I data from July 1987 to the present. Similar data from AMSR-E were also generated from June 2002 up to the present. The relatively long overlap of AMSR-E and SSM/I data enabled detailed examination of the consistency of the two data sets when the same ice algorithm is applied and the brightness temperatures from the same sensors are inter-calibrated. The resulting ice concentration maps were basically identical except at the ice margins where resolution effects are apparent. The enhanced SSM/I data during the period of overlap are in turn used to enhance data from the other SSM/I sensors and subsequently those from SMMR sensor. We have shown that the time series generated shows good consistency despite apparent differences in the physical characteristics of the different satellite sensors that provided the data.

It is encouraging that the agreement between AMSR-E and SSM/I ice extents and area data is as good as indicated in the plots presented despite the vast differences in resolution. The use of ice concentration is expected to take care of the resolution problem but not completely especially in the estimates of ice extent. As indicated the data with lower resolution will find the ice edge further away from the pack than the one with higher resolution. Although the same algorithm is applied on the two data sets, the fields of view and side lobes of the two sensors are different and hence the observed radiances from the two sensors cannot be identical even if the calibration of each is perfect. Also, the exact locations of 15% ice edge as observed by the different sensors are not expected to be same. In addition to differences in resolution, there is also differences in revisit time of the different sensors: one (SSM/I) crossing the equatorial line at about 10 am while the other (AMSR-E) at about 1 pm. Since the ice cover is dynamic and the ice edge can easily be altered by winds, the ice edge location can be significantly changed within the three hour difference.

Our analysis show that errors (or biases) in ice extent have to be considered when combining data from different sensors with different resolutions. This already assumes that the ice concentrations are derived in a similar fashion and the masking for open water, land and ice/ocean boundaries are similar if not identical. There are also mismatches in the estimates for ice area but they are basically small and negligible. For trend studies of ice extent, the sole use of SMMR and SSM/I data is recommended instead of using the more accurate AMSR-E data when the latter is available to avoid error associated with a slight bias caused by mismatches in resolution. For trend studies of ice area, such bias is almost negligible and the use of AMSR-E data has the advantage of providing more accurate results. However, because of the short record length of the latter (about 5 years), interpretation of trend results will likely be the same in both cases.

Acknowledgement: I wish to acknowledge the excellent programming and analysis support provided by Robert Gersten of RSIS. The project was supported by the NASA's Cryospheric Sciences and EOS programs.

REFERENCES

Bjorgo, E. , O.M. Johannessen, and M.W. Miles, "Analysis of merged SSMR-SSM/I time series of Arctic and Antarctic sea ice parameters 1978-1995," *Geophys. Res. Lett*., Vol. 24, pp. 413-416, 1997.

Cavalieri, D.J., P. Gloersen, W.J. Campbell, Determination of sea ice parameters with the Nimbus7 SMMR, J. Geophys Res., 89, 5355-5369, 1984.

Cavalieri, D.J., P. Gloersen, C. Parkinson, J. Comiso, and H.J. Zwally, Observed hemispheric asymmetry in global sea ice changes, *Science, 278*(7), 1104-1106,1997.

Cho, K., N. Sasaki, H. Shimoda, T. Sakata and F. Nishio, Evaluation and improvement of SSM/I sea ice concentration algorithms for the Sea of Okhotsk, J. Remote Sensing of Japan, 16(2), 47-58, 1996.

Colony, R. and A. Thorndike, Sea ice motion as a drunkard's walk, J. Geophys. Res, 90, 965-974, 1985.

Comiso, J. C., Sea ice microwave emissivities from satellite passive microwave and infrared observations, *J. Geophys. Res., 88*(C12), 7686-7704, 1983.

Comiso, J. C., Characteristics of winter sea ice from satellite multispectral microwave observations, *J. Geophys. Rev., 91*(C1), 975-994, 1986.

Comiso, J.C., SSM/I Concentrations using the Bootstrap Algorithm, *NASA RP, 1380*, 40pp, 1995.

Comiso, J. C., A rapidly declining Arctic perennial ice cover, *Geophys Res. Letts., 29(20), 1956, doi:10.1029/2002GL015650*, 2002.

Comiso, J.C., Sea ice algorithm for AMSR-E, *Rivista Italiana di Telerilevamento (Italian Journal of Remote Sensing), 30/31*, 119-130, 2004.

Comiso, J.C., and A.L. Gordon, The Cosmonaut Polynya in the Southern Ocean: Structure and variability, *J. Geophys. Res., 101*(C8), 18297-19313, 1996.

Comiso, J. C. and F. Nishio, Trends in the sea ice cover using enhanced and compatible AMSR-E, SSM/I, and SMMR data, J. Geophys. Res. (2007, submitted).

Comiso, J. C. and C. W. Sullivan, Satellite microwave and in-situ observations of the Weddell Sea ice cover and its marginal ice zone, *J. Geophys. Res., 91*(C8), 9663-9681, 1986.

Comiso, J.C., and K. Steffen, Studies of Antarctic sea ice concentrations from satellite data and their applications, *J. Geophys. Res., 106*(C12), 31361-31385, 2001.

Comiso, J. C., S. F. Ackley, and A. L. Gordon, Antarctic Sea Ice Microwave Signature and their correlation with In-Situ Ice Observations, *J. Geophys. Res., 89*(C1), 662-672,1984.

Comiso, J. C., D. J. Cavalieri, and T. Markus, Sea ice concentration, ice temperature, and snow depth, using AMSR-E data, *IEEE TGRS, 41(2),* 243-252, 2003.

Comiso, J.C., D. Cavalieri, C. Parkinson, and P. Gloersen, Passive microwave algorithms for sea ice concentrations, *Remote Sensing of the Env., 60*(3), 357-384, 1997.

Comiso, J.C., P. Wadhams, L.T. Pedersen, and R. Gersten, The seasonal and interannual variability of the Odden and a study of environmental effects, *J. Geophys. Res., 106*(C5), 9093-9116, 2001.

Eicken, H., M.A. Lange, and G.S. Dieckmann, Spatial variability of sea-ice properties in the northwestern Weddell Sea, J. Geophys. Res., 96, 10,603-10,615, 1991

Eppler, D., M.R. Anderson, D.J. Cavalieri, J.C. Comiso, L.D. Farmer, C. Garrity, P. Gloersen, T., Grenfell, M. Hallikainen, A.W. Lohanick, C. Maetzler, R.A. Melloh, I. Rubinstein, C.T. Swift, C. Garrity, "Passive microwave signatures of sea ice," Chapter 4, *Microwave Remote Sensing of Sea Ice*, (ed. by Frank Carsey), American Geophysical Union, Washington, D.C., 47-71, 1992.

Gloersen P., W. Campbell, D. Cavalieri, J. Comiso, C. Parkinson, H.J. Zwally, Arctic and Antarctic Sea Ice, 1978-1987: Satellite Passive Microwave Observations and Analysis, *NASA Spec. Publ. 511*, 1992.

Grenfell, T.C. 1992.Surface-based passive microwave studies of multiyear ice. *J. Geophys. Res.*, **97**(C3), 3485-3501.

Kumerow, C, On the accuracy of the Eddington approximation for radiative transfer in the microwave frequencies," *J. Geophys. Res*, Vol. 98, pp. 2757- 2765, 1993.

Markus, T and D. Cavalieri, An enhancement of the NASA team sea ice algorithm, IEEE Trans. Geosci. Remote Sensing, 38, 1387-1398, 2000.

Matzler, C., R. O. Ramseier, and E. Svendsen, "Polarization effects in sea ice signatures," *IEEE J. Oceanic Engineering*, Vol. OE-9, pp. 333-338, 1984.

Parkinson, C.L., D.J Cavalieri, P. Gloersen, H.J. Zwally, and J.C. Comiso, Arctic sea ice

extents, areas, and trends, 1978-1996, *J. Geophys. Res.*, *104*(C9), 20837-20856, 1999.
Serreze, M.C., and Co-authors, Observational evidence of recent chang in the northern high-latitude environment, *Climatic Change, 46*, 159-207, 2000.
Steffen, K., D. J. Cavalieri, J. C. Comiso, K. St. Germain, P. Gloersen, J. Key, and I. Rubinstein, "The estimation of geophysical parameters using Passive Microwave Algorithms," Chapter 10, *Microwave Remote Sensing of Sea Ice*, (ed. by Frank Carsey), American Geophysical Union, Washington, D.C., 201-231, 1992.
Stroeve, J.C., M.C., Serreze, F. Fetterer, T. Arbetter, M. Meier, J. Maslanik and K. Knowles, Tracking the Arctic's shrinking ice cover: Another extreme September minimum in 2004, *Geophys. Res. Lett. 32*, doi:10.1029/2004GL021810, 2004.
Svendsen, E., C. Matzler, T.C. Grenfell, "A model for retrieving total sea ice concentration from a spaceborne dual-plarized passive microwave instrument operating near 90 GHz," *Int. J. Rem. Sens.*, Vol. 8, pp. 1479-1487, 1987.
Swift, C.T., L.S. Fedor, and R.O. Ramseier, An algorithm to measure sea ice concentration with microwave radiometers, J. Geophys. Res., 90(C1), 1087-1099, 1985.
Tucker, W.B., D.K. Perovich, and A.J. Gow, "Physical properties of sea ice relevant to remote sensing," Chapter 2, *Microwave Remote Sensing of Sea Ice*, (ed. by Frank Carsey), American Geophysical Union, Washington, D.C., 9-28, 1992.
Vant, M.R., R.B. Gray, R.O. Ramseier, and V. Makios. 1974. Dielectric properties of fresh and sea ice at 10 and 35 GHz, *J. Applied Physics*, *45(11)*, 4712-4717.
Weeks, W.F., and S. F. Ackley, The growth, structure and properties of sea ice, *The Geophysics of Sea Ice*, edited by N. Unterstiener, pp. 9-164, *NATO ASI Ser.B*, vol. 146, Plenum, New York, 1986.
Worby, A. P., and J. C. Comiso, Studies of Antarctic sea ice edge and ice extent from satellite and ship observations, *Remote Sensing of the Environment*, *92*(1), 98-111, 2004.
Zwally, H.J., J.C. Comiso, C. Parkinson, D. Cavalieri, P. Gloersen, Variability of the Antarctic sea ice cover, *J. Geophys. Res.* 107(C5), 1029-1047, 2002.
Zwally, H. J., J. C. Comiso, C. L. Parkinson, W. J. Campbell, F. D. Carsey, and P. Gloersen, Antarctic Sea Ice 1973-1976 from Satellite Passive Microwave Observations, *NASA Spec. Publ. 459*, 1983.